

# Electron-electron interactions in graphene bilayers

Fan Zhang,<sup>1</sup> Hongkim In,<sup>1</sup> Marco Polini,<sup>2</sup> and A.H.MacDonald<sup>1</sup>

<sup>1</sup>Department of Physics, University of Texas at Austin, Austin TX 78712, USA

<sup>2</sup>NEST-CNR-INFM and Scuola Normale Superiore, I-56126 Pisa, Italy

Electrons most often organize into Fermi-liquid states in which electron-electron interactions play an inessential role. A well known exception is the case of one-dimensional (1D) electron systems (1DES). In 1D the electron Fermi-surface consists of points, and divergences associated with low-energy particle-hole excitations abound when electron-electron interactions are described perturbatively. In higher space dimensions, the corresponding divergences occur only when Fermi lines or surfaces satisfy idealized nesting conditions. In this article we discuss electron-electron interactions in 2D graphene bilayer systems which behave in many ways as if they were one-dimensional, because they have Fermi points instead of Fermi lines and because their particle-hole energies have a quadratic dispersion which compensates for the difference between 1D and 2D phase space. We conclude, on the basis of a perturbative RG calculation similar to that commonly employed in 1D systems, that interactions in neutral graphene bilayers can drive the system into a strong-coupling broken symmetry state with layer-pseudospin ferromagnetism and an energy gap.

Recent progress in the isolation of nearly perfect single and multilayer graphene sheets<sup>1,2,3,4</sup> has opened up a new topic in two-dimensional electron systems (2DES) physics. There is to date little unambiguous experimental evidence that electron-electron interactions play an essential role in the graphene family of 2DES's. However, as pointed out by Min et al.<sup>5</sup> graphene bilayers near neutrality should be particularly susceptible to interaction effects because of their peculiar massive-chiral band Hamiltonian, which has an energy-splitting between valence and conduction bands that vanishes at  $k = 0$  and grows quadratically with  $k = |\mathbf{k}|$ :

$$H_B = \sum_{\mathbf{k}} \frac{\hbar^2 k^2}{2m} c_{\mathbf{k}0}^\dagger \cos(J_{\mathbf{k}}) c_{\mathbf{k}0} + \sin(J_{\mathbf{k}}) c_{\mathbf{k}0}^\dagger c_{\mathbf{k}} : \quad (1)$$

In Eq. (1) the  $c$ 's are Pauli matrices and the Greek labels refer to the two bilayer graphene sublattice sites, one in each layer, which do not have a neighbor in the opposite graphene layer. (See Fig. 1.) The other two sublattice site energies are repelled from the Fermi level by interlayer hopping and irrelevant at low energies. It is frequently useful to view quantum two-level layer degree of freedom as a pseudospin. The  $J = 2$  pseudospin

chirality of bilayer graphene contrasts with the  $J = 1$  chirality<sup>1,7</sup> of single-layer graphene and is a consequence of the two-step process in which electrons hop between low-energy sites via the high-energy sites. The massive-chiral band-structure model applies at energies smaller than the interlayer hopping scale<sup>4</sup>  $\sim 0.3$  eV but larger than the trigonal-warping scale<sup>4</sup>  $\sim 0.03$  eV below which direct hopping between low-energy sites plays an essential role. The body of this paper concerns the role of interactions in the massive-chiral model; we return at the end to explain the important role played by trigonal warping.

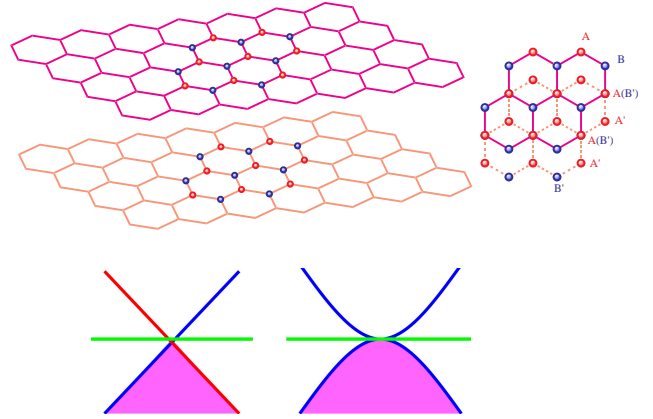


FIG. 1: Bilayer graphene lattice structure and electronic structure. The massive chiral fermion model describes the low-energy sites in a AB-stacked graphene bilayer, those atom sites (top layer B sites and bottom layer A sites) which do not have a neighbor in the opposite layer. The conduction and valence bands touch at the Brillouin-zone corner wavevectors, taken as zero-momentum in continuum model theories, and separate quadratically with increasing wavevector. In a 1DES left and right going electrons cross the Fermi energy at a single point. In this figure the momentum of right-going (left-going) electrons is plotted relative to  $+k_F$  ( $-k_F$ ) where  $k_F$  is the Fermi wavevector.

Similarities and differences between graphene bilayers and 1DES are most easily explained by temporarily neglecting the spin, and in the case of graphene also the additional valley degree of freedom. As illustrated in Fig. 1 in both cases the Fermi sea is point-like and there is a gap between occupied and empty free-particle states which grows with wavevector, linearly in the 1DES case. These circumstances are known to support a mean-field broken symmetry state in which phase coherence is established between conduction and valence band states for arbitrarily weak repulsive interactions. In the case

of 1DES, the broken symmetry state corresponds physically to a charge density-wave (CDW) state, while in the case of bilayer graphene<sup>5</sup> it corresponds to a state in which charge is spontaneously transferred between layers. This mean-field theory prediction is famously incorrect in the 1DES case, and the origin of the failure can be elegantly identified<sup>8,9</sup> using a perturbative renormalization group (PRG) approach. We show below that when applied to bilayer graphene, the same considerations lead to a different conclusion.

The reliability of the mean-field theory prediction<sup>5</sup> of a weak-interaction instability in bilayer graphene can be systematically assessed using PRG<sup>8</sup>. We outline the main steps in the application of this analysis to bilayer graphene in the main text, pointing out essential differences compared to the 1DES case. Details are provided in the supplementary material. We assume short-range interactions between electrons in the same (S) and different (D) layers.

The PRG analysis centers on the four-point scattering function defined in terms of Feynman diagrams in Fig. 2. Since the Pauli exclusion principle implies that (in the spinless valleyless case) no pair of electrons can share the same 2D position unless they are in opposite layers, intralayer interactions cannot influence the particles; there is therefore only one type of interaction generated by the RG flow, interactions between electrons in opposite layers with the renormalized coupling parameter  $V_D$ . The direct and exchange first order processes in Fig. 2 have the values  $V_D$  and 0 respectively where  $V_D$  is the bare coupling parameter.

The PRG analysis determines how  $V_D$  is renormalized in a RG procedure in which fast (high energy) degrees of freedom are integrated out and the fermion fields of the slow (low energy) degrees of freedom are rescaled to leave the free-particle action invariant. The effective interaction  $V_D$  is altered by coupling between low and high energy degrees of freedom. At one loop level this interaction is described<sup>8</sup> by the three higher order diagrams labeled ZS, ZS', and BCS in Fig. 2. The internal loops in these diagrams are summed over the high-energy labels. In the case of 1DES the ZS loop vanishes and the ZS' and BCS diagrams cancel, implying that the interaction strengths do not flow to large values and that neither the CDW repulsive interaction nor the BCS attractive interaction instabilities predicted by mean-field theory survive the quantum fluctuations they neglect. The key message of this paper is summarized by two observations about the properties of these one-loop diagrams in the bilayer graphene case; i) the particle-particle (BCS) and particle-hole (ZS, ZS') loops have the same logarithmic

divergences as in the 1DES case in spite of the larger space dimension and ii) the ZS loop, which vanishes in the 1DES case, is finite in the bilayer graphene case and the BCS loop vanishes instead. Both of these changes are due to a layer pseudospin triplet contribution to the single-particle Green's function as we explain below. The net result is that interactions flow to strong coupling even more strongly than in the mean-field approximation. The following paragraphs outline key steps in the calculations which support these conclusions.

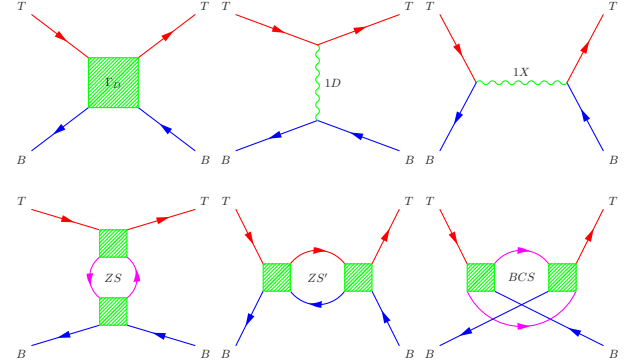


FIG. 2: Four-point scattering function for bilayer graphene. The 1st diagram is the renormalized interaction while the 2nd and 3rd ones are the direct and exchange bare interactions, respectively. The following diagrams are the one-loop diagrams labelled ZS, ZS' and BCS. The external and internal Green's function labels refer to layer in the case of graphene and to chirality in the case of 1DES.

An elementary calculation shows that the single-particle Matsubara Green's function corresponding to the Hamiltonian in Eq. (1) is

$$\mathcal{G}(\mathbf{k}; i!_n) = \begin{pmatrix} \mathcal{G}_s(\mathbf{k}; i!_n) & \mathcal{G}_t(\mathbf{k}; i!_n) e^{i\mathbf{T} \cdot \mathbf{k}} \\ \mathcal{G}_t(\mathbf{k}; i!_n) e^{i\mathbf{T} \cdot \mathbf{k}} & \mathcal{G}_s(\mathbf{k}; i!_n) \end{pmatrix} \quad (2)$$

where

$$\mathcal{G}_{s;t}(\mathbf{k}; i!_n) = \frac{1}{2} \frac{1}{i!_n - !_k} \frac{1}{i!_n + !_k} ; \quad (3)$$

and  $!_k = \mathbf{k} \cdot \mathbf{k} = k^2 = 2m^2$ . The pseudospin-singlet component of the Green's function  $\mathcal{G}_s$ , which is diagonal in layer index, changes sign under frequency inversion whereas the triplet component  $\mathcal{G}_t$ , which is off-diagonal, is invariant.

The loop diagrams are evaluated by summing the product of two Green's functions (corresponding to the two arms of the Feynman diagram loops) over momentum and frequency. The frequency sums are standard and yield  $(= (k_B T)^{-1})$

$$\begin{aligned} \frac{1}{\sim 2} \sum_{!_n}^X \mathcal{G}_{s;t}^2(i!_n) &= \frac{\tanh(\beta k/2)}{4 k} \sum_{!_0}^X \frac{1}{4 k} \\ \frac{1}{\sim 2} \sum_{!_n}^X \mathcal{G}_s(i!_n) \mathcal{G}_t(i!_n) &= 0 \end{aligned} \quad (4)$$

We replace the bare Coulomb interactions by short-range momentum-independent interactions<sup>8</sup> by evaluating them at typical momentum transfers at the model's high-energy limit. We believe that this approximation is not serious because of screening.

where  $k$  is the momentum label shared by the Green's functions. Note that the singlet-triplet product sum vanishes in the low-temperature limit in which we are interested. Each loop diagram is multiplied by appropriate interaction constants (discussed below) and then integrated over high energy momentum labels up to the massive chiral fermion model's ultraviolet cutoff:

$$\int_{s < k < \Lambda} \frac{d^2 k}{(2\pi)^2} \frac{\tanh(k/2)}{4k} \ln(s) : \quad (5)$$

where  $\Lambda = m/2\pi^2$  is the graphene bilayer density-of-states. Because  $\Lambda/k^2$ , this integral grows logarithmically when the high-energy cutoff is scaled down by a factor of  $s$  in the RG transformation, exactly like 1DES. This rather surprising property of bilayer graphene is directly related to its unusual band structure with Fermi points rather than Fermi lines and quadratic rather than linear dispersion.

The key differences between bilayer graphene and the 1DES appear upon identifying the coupling factors which are attached to the loop diagrams. The external legs in the scattering function Feynman diagrams (Fig. 2) are labeled by layer index ( $T$  = top layer and  $B$  = bottom layer) in bilayer graphene. The corresponding labels for the 1DES are chirality ( $R$  = right-going and  $L$  = left-going); we call these interaction labels when we refer to the two cases generically. Since only opposite layer interactions are relevant, all scattering functions have two incoming particles with opposite layer labels and two outgoing particles with opposite layer labels. In the  $ZS$  loop, at the upper vertex the incoming and outgoing  $T$  particles induce a  $B$  particle-hole pair in the loop while the incoming and outgoing  $B$  particles at the lower vertex induce a  $T$  particle-hole pair. Since the particle-hole pairs must annihilate each other, there is a contribution only if the single-particle Green's function is off-diagonal in interaction labels. This loop can be thought of as screening  $V_D$ ; the sign of the screening contribution is opposite to normal, enhancing the bare interlayer interaction, because the polarization loop involves layer pseudospin triplet propagation. (See Eq. (4).) This contribution is absent in the 1DES case because propagation is always diagonal in interaction labels. The  $ZS'$  channel corresponds to repeated interaction between a  $T$  particle and a  $B$  hole. This loop diagram involves only particle-propagation that is diagonal in interaction labels and its evaluation in the graphene bilayer case therefore closely follows the 1DES calculation. This is the channel responsible for the 1DES mean-field CDW instability in which coherence is established between  $R$  and  $L$  particles. In both graphene bilayer and 1DES cases it has the effect of enhancing repulsive interactions. The  $BCS$  loop corresponds to repeated interaction between the two incoming particles. In the 1DES case the contribution from this loop which enhances attractive interactions, cancels the  $ZS'$  contribution, leading to marginal interactions and Luttinger liquid behavior. In the graphene bilayer case however, there is an additional contribution to the

TABLE I: Summary of contrasting the contributions (in units of the related density-of-states) of the three one-loop diagrams in 1DES and graphene bilayer cases

diagrams	$ZS$	$ZS'$	$BCS$	one-loop
1DES	0	$u^2 \ln(s)$	$u^2 \ln(s)$	0
graphene bilayer	$\frac{1}{2} \frac{V_D}{D} \ln(s)$	$\frac{1}{2} \frac{V_D}{D} \ln(s)$	0	$\frac{2}{D} \ln(s)$

$BCS$  loop contribution in which the incoming  $T$  and  $B$  particles both change interaction labels before the second interaction. This contribution is possible because of the triplet component of the particle propagation and, in light of Eq. (4), gives a  $BCS$  loop contribution with a sign opposite to the conventional one. Summing both terms, it follows that the  $BCS$  loop contribution is absent in the graphene bilayer case. These results are summarized in Table I and imply that at one loop level

$$D' = \frac{V_D}{1 - V_D \Lambda} \ln(s) : \quad (6)$$

The interaction strength diverges when  $V_D \Lambda = 1 = \ln(s)$ , at half the mean-field theory critical interaction strength. Taking guidance from the mean-field theory<sup>5</sup>, the strong coupling state is likely a pseudospin ferromagnet which has an energy gap and spontaneous charge transfer between layers.

A number of real-world complications which have to be recognized in assessing the experimental implications of these results. First of all, electrons in real graphene bilayers carry spin and valley as well as layer pseudospin degrees of freedom. This substantially complicates the PRG analysis since many different types of interactions are generated by the RG flow. When one spin degree of freedom is considered three types of interactions have to be recognized,  $s$ ,  $D$ , and  $x$ .  $s$  couples electrons with the same flavor and  $D$  electrons with different flavors, while  $x$  is the exchange counterpart of  $D$ . The bare value of the exchange part of  $D$  (the direct part of  $x$ ) is of course zero since the Coulomb interaction is flavor independent, but higher order contributions are nonzero if triplet electron propagation is allowed. Correspondingly, when both spin and valley degrees of freedom are acknowledged the interaction parameters are  $SSD$ ,  $SDS$ ,  $SDD$ ,  $DSS$ ,  $DSD$ ,  $DDS$ ,  $DDD$ ,  $XSD$ ,  $XDS$ , and  $XDD$  (see supplementary material). The labels refer from left to right to sublattice pseudospin, real spin, and valley degrees of freedom.  $SSS$  is absent due to Pauli exclusion principle while  $XSS$  is just

<sup>5</sup> Mean-field theory is equivalent to a single-loop PRG calculation in which only one particle-hole channel is retained. For the drawing conventions of Fig. 2 the susceptibility which diverges at the pseudospin ferromagnet phase boundary is obtained by closing the scattering function with  $z$  vertices at top and bottom, so the appropriate particle-hole channel is the  $ZS$  channel not the  $ZS'$  channel.

Due to the fermionic antisymmetry between outgoing particles. The one loop flow of these ten interaction parameters is described in the supplementary material. We find that the renormalized interactions diverge near  $V_D \rightarrow 0$ :  $\ln(s)$ . The instability tendency is therefore somewhat enhanced by the spin and the valley degrees of freedom.

Next we must recognize that the massive chiral fermion model applies only between trigonal-warping and inter-layer hopping energy scales. Appropriate values for  $\ln(s)$  in the RG flows are therefore at most around 2:3 (see supplementary material) in bilayer graphene, compared to the unlimited values of the chiral-fermion model. When combined with estimates of the bare interaction strengths (see supplementary material), this limit on interaction flow suggests that spontaneous gaps are likely in suspended bilayer graphene samples, and much less likely for graphene bilayers on substrates.

Gaps do appear in bilayer graphene even when electron-electron interactions are neglected, provided that an external potential difference  $V$  is applied between the layers. The potential adds a single-particle term  $V^2=2$  to the single-particle Hamiltonian, breaks

inversion symmetry, and transfers charge<sup>10,11,12,13</sup> between layers. This interesting property is in fact the basis of one strategy currently being explored in the effort to make useful electronic devices<sup>14,15</sup> out of graphene 2DES's. Even if gaps do not appear spontaneously in real bilayer graphene samples, it is clear from the present work that interesting many-body physics beyond that captured by commonly used electronic-structure-theory approximations (LDA or GGA approximations for example), must play at least a quantitative role in determining gap growth with  $V$ . As graphene bilayer sample quality improves, we expect that it will be possible to explore this physics experimentally with ARPES, tunneling, and transport probes.

#### Acknowledgments

This work has been supported by the Welch Foundation and by the National Science Foundation under grant DMR-0606489. AHM gratefully acknowledges helpful discussion with R. Shankar and I. Alek.

---

Electronic address: zhangfan@physics.utexas.edu

- <sup>1</sup> Ando, T. Theory of electronic states and transport in carbon nanotubes. *J. Phys. Soc. Jpn.* 74, 777-817 (2005).
- <sup>2</sup> Geim, A. K. & Novoselov, K. S. The rise of graphene. *Nature Mater.* 6, 183 (2007).
- <sup>3</sup> Geim, A. K. & MacDonald, A. H. Graphene: Exploring carbon at land. *Phys. Today* 60 (8), 35 (2007).
- <sup>4</sup> Castro Neto, A. H., Guinea, F., Peres, N. M. R., Novoselov, K. S. & Geim, A. K. The electronic properties of graphene. *Rev. Mod. Phys.* 81, 109 (2009).
- <sup>5</sup> Min, H., Borghi, G., Polini, M. & MacDonald, A. H. Pseudospin magnetism in graphene. *Phys. Rev. B* 77, 041407(R) (2008).
- <sup>6</sup> McCann, E. & Fal'ko, V. I. Landau-level degeneracy and quantum hall effect in a graphite bilayer. *Phys. Rev. Lett.* 96, 086805 (2006).
- <sup>7</sup> Barlas, Y., Pereg-Barnea, T., Polini, M., Asgari, R. & MacDonald, A. H. Chirality and correlations in graphene. *Phys. Rev. Lett.* 98, 236601 (2007).
- <sup>8</sup> Shankar, R. Renormalization-group approach to interacting fermions. *Rev. Mod. Phys.* 66, 129 (1994).
- <sup>9</sup> Giamarchi, T. *Quantum Physics in One Dimension* (Clarendon Press, Oxford, 2003).
- <sup>10</sup> Ohta, T., Bostwick, A., Seyller, T., Hom, K. & Rotenberg, E. Controlling the electronic structure of bilayer graphene. *Science* 313, 951 (2006).
- <sup>11</sup> Castro, E. V. et al., Biased bilayer graphene: semiconductor with a gap tunable by the electric field effect. *Phys. Rev. Lett.* 99, 216802 (2007).
- <sup>12</sup> McCann, E. A symmetry gap in the electronic band structure of bilayer graphene. *Phys. Rev. B* 74, 1403 (2006).
- <sup>13</sup> Min, H., Sahu, B., Banerjee, S. K. & MacDonald, A. H. Ab initio theory of gate induced gaps in graphene bilayers. *Phys. Rev. B* 75, 155115 (2007).
- <sup>14</sup> Oostinga, J. B., Heersche, H. B., Liu, X., Morpurgo, A. F. & Vandersypen, L. M. K. Gate-induced insulating state in bilayer graphene devices. *Nature Mater.* 7, 151 (2008).
- <sup>15</sup> Martin, J. Scanning single electron transistor microscopy on graphene. *Bull. Am. Phys. Soc.* 54 (1), 191 (2009).

## Supplementary Information for "Electron-electron interactions in graphene bilayers"

Fan Zhang<sup>1</sup>, Hongkim Min<sup>1</sup>, Marco Polini<sup>2</sup> and A.H. MacDonald<sup>1</sup><sup>1</sup>Department of Physics, University of Texas at Austin, Austin TX 78712, USA<sup>2</sup>NEST-CNR-INFM and Scuola Normale Superiore, I-56126 Pisa, Italy

In this supplementary information, we summarize the Green's function technique, detail the diagrammatic perturbation theory calculations, and explain them any interaction channels generated by the RG flow when spin and valley degrees of freedom are included. We also discuss the bare interactions and the important trigonal-warping effect.

## I. GREEN'S FUNCTIONS AND FREQUENCY SUMS

The low-energy effective Hamiltonian of a graphene bilayer is a momentum  $q$ -dependent  $2 \times 2$  matrix of the following form :

$$\mathcal{H} = B \cdot \beta \quad ; \quad (1)$$

where  $\beta$  is the Pauli matrix vector,  $\beta_j = \sigma_j = \hbar^2 q^2 = 2m$ , and the orientation angle of  $B$  is twice the orientation angle of  $q$  ( $\phi_q$ ). (This property is often expressed by saying that the model has layer pseudospin chirality<sup>1,2</sup>  $J=2$ .) The pseudospin degree of freedom upon which the operator acts represents the layer in which an electron resides. Eigenstates of  $\mathcal{H}$  are coherent linear combinations of amplitudes in both layers. The finite temperature Green's function at Matsubara fermion frequency  $i!_n$  and wavevector  $q$  is given by

$$\mathcal{G}(i!_n) = [i!_n - \mathcal{H} = \hbar]^{-1} = \mathcal{G}_s(i!_n) + \mathcal{G}_t(i!_n) \quad (2)$$

where

$$\mathcal{G}_{s/t}(i!_n) = \frac{1}{2} \frac{1}{i!_n - \beta_q} \frac{1}{i!_n + \beta_q} \quad ; \quad (3)$$

in  $B = \beta_j$ , the "s" and "t" subscripts denote singlet and triplet contributions respectively, and we have chosen  $\beta_q = 0$  to address the properties of an electrically neutral bilayer. Note that  $\mathcal{G}_s(i!_n) = \mathcal{G}_s(i!_n)$  whereas  $\mathcal{G}_t(i!_n) = \mathcal{G}_t(i!_n)$ . Using the property that  $n = (\cos(2\phi_q); \sin(2\phi_q); 0)$  we obtain the following explicit form for the  $2 \times 2$  Green's function matrix:

$$\mathcal{G}(i!_n) = \begin{pmatrix} \mathcal{G}_s(i!_n) & \mathcal{G}_t(i!_n)e^{2i\phi_q} \\ \mathcal{G}_t(i!_n)e^{2i\phi_q} & \mathcal{G}_s(i!_n) \end{pmatrix} \quad ; \quad (4)$$

The off-diagonal triplet component captures processes in which free electrons propagate from one layer to the other. Evaluation of the loop diagrams which appear in the RG calculation described in the main text requires frequency sums to be performed for products of two Green's functions. These are given by

$$\frac{1}{\hbar^2} \sum_{!_n} \mathcal{G}_{s/t}^2(i!_n) = \frac{\tanh(\beta_q/2)}{4\beta_q} \frac{1}{\beta_q} \quad ; \quad \frac{1}{\hbar^2} \sum_{!_n} \mathcal{G}_s(i!_n) \mathcal{G}_t(i!_n) = 0 \quad (5)$$

## II. SPIN PSEUDOSPINS AND DISTINCT INTERACTION PARAMETERS

In the low-energy continuum model of bilayer graphene electrons carry spin, and both layer and valley pseudospin labels. In a scattering event, both the two incoming and two outgoing particles can therefore have one of eight labels and the general scattering function therefore has  $8^4$  possible low-energy long-wavelength values. The number of distinct coupling constants in the RG flow equations is much smaller, however, because many values are zero and others are related to each other by symmetry. One simplification is that interactions conserve spin, and both layer and valley pseudospin, at each vertex. Interactions are however dependent on whether the interacting particles are in the same (S) or in different (D) layers. The internal loops in the perturbative RG calculation contain two fermion propagator (Green's function) lines. These propagators conserve both spin and valley pseudospin, but as we have seen above, not the layer pseudospin. It is clear then that the incoming and outgoing total spin must be preserved for



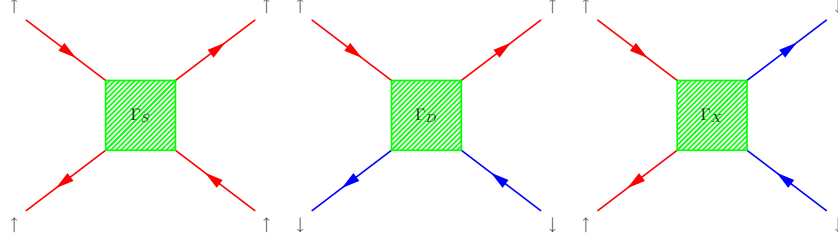


FIG. 1: Electron-electron scattering processes for a system with one pseudospin-1/2 degree of freedom.

real spin and for the valley pseudospin, but the layer pseudospin case requires a more elaborate consideration. From Eq. (4) we see that a phase factor  $e^{2i\varphi}$  is gained when the propagator transfers electrons between layer index with the + for top to bottom evolution and the - for bottom to top. Unless these transfers enter an equal number of times in each direction, the integrand in a Feynman diagram will contain a net phase factor related to chirality and vanish under momentum integration. The total layer pseudospin is therefore also conserved in collisions.

In identifying distinct coupling constants, we start with the simplest case in which the valley and spin labels are absent. There are then three possibilities, as illustrated in Fig. 1. When the two incoming pseudospins are parallel ( $\Gamma_S$  in Fig. 1), the outgoing pseudospins must also be parallel. Because of Fermi statistics interchanging the outgoing lines in  $\Gamma_S$  changes the diagram's sign. Since the diagram is invariant under this operation, it must vanish. The second possibility is opposite incoming pseudospins, which requires opposite outgoing pseudospins in one of the two configurations labelled by  $\Gamma_D$  and  $\Gamma_X$  in Fig. 1. In this case Fermi statistics implies that  $\Gamma_D = \Gamma_X$ . It follows that the only distinct interaction parameter is  $\Gamma_D$ .

If more than one pseudospin is present, we have to recognize more separate interacting processes. For example, for systems with two relevant pseudospins, the interaction parameters can be labeled in the same way as in Fig. 1 but by doublets which account for the different pseudospins separately. Two pseudospin interactions might include  $\Gamma_{SD}$ ,  $\Gamma_{DS}$ ,  $\Gamma_{DD}$  and  $\Gamma_{XD}$  (see Fig. 2) for example. In models for which propagators and interactions preserve all pseudospin labels, we would have  $\Gamma_{XD} = 0$  since all pseudospin flavors are preserved along each fermion line. For graphene bilayers, however, we must keep  $\Gamma_{XD} \neq 0$  because the layer pseudospin has triplet propagation. Following this line of argument, we conclude that in graphene bilayers, with its three different pseudospins, there are ten distinct non-zero interaction parameters:  $\Gamma_{SSD}$ ,  $\Gamma_{SDS}$ ,  $\Gamma_{SDD}$ ,  $\Gamma_{DSS}$ ,  $\Gamma_{SDS}$ ,  $\Gamma_{DDS}$ ,  $\Gamma_{DDD}$ ,  $\Gamma_{XSD}$ ,  $\Gamma_{XDS}$  and  $\Gamma_{XDD}$ , where the first label refers to layer pseudospin, and the following labels to real spin and valley.

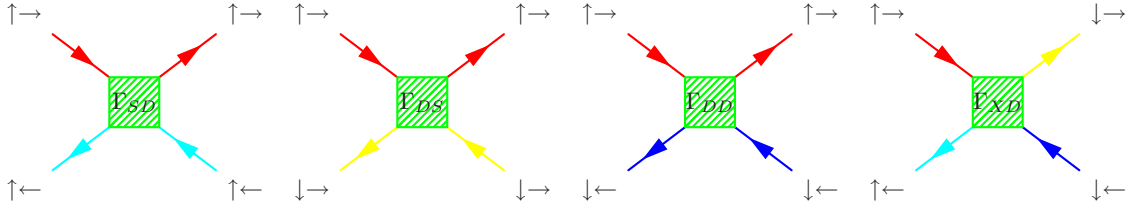


FIG. 2: Distinct interaction channels for systems with two pseudospin-1/2 degrees of freedom. In this figure the first spin is denoted by  $j''i$  or  $j\#i$  while the second by  $j'i$  or  $j_i$ . The one-dimensional electron gas system can be viewed as being in this class if the chirality index is regarded as a pseudospin.

### III. PRG ANALYSIS FOR SPINLESS AND VALLEYLESS GRAPHENE BILAYERS

The one-loop correction to the interlayer interaction  $\Gamma_D$  can be calculated using the following ZS, ZS' and BCS diagrams<sup>4</sup>. Since  $\Gamma_D$  (with bare value  $V_D$ ) is the only interaction parameter as we explained previously, the propagator labels of the internal loops must be distributed accordingly. We label the external legs in the scattering diagrams by their layer indices ( $T$  = top layer and  $B$  = bottom layer). The corresponding labels for the 1DES are chirality ( $R$  = right-going and  $L$  = left going).

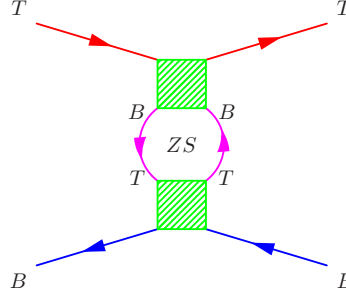


FIG. 3: ZS loop correction in the one-loop perturbative RG calculation.

In the ZS loop shown in Fig. 3, at the upper vertex the incoming and the outgoing T particles induce a B particle-hole pair in the loop while the incoming and outgoing B particles at the lower vertex induce a T particle-hole pair. The corresponding labels in the 1DES case are L, R for left and right chirality. This correction survives in the bilayer case only because the single-particle Green's function has a triplet contribution [see Eq. (5)] which is off-diagonal in layer index. The ZS contribution is absent in the 1DES case<sup>4,5</sup> because propagation is always diagonal in interaction labels. Here we find

$$\chi_D^{ZS} = \frac{2_D}{h^2} \int_{-s}^s \frac{d^2 q}{(2\pi)^2} \chi \mathcal{G}_t^2(\mathbf{q}; i\epsilon_n) = \frac{2_D}{h^2} \int_{-s}^s \frac{d^2 q}{(2\pi)^2} \frac{\tanh(\epsilon_q/2)}{4\epsilon_q} = \frac{1}{2} \frac{2_D}{h^2} \rho_0 \ln(s); \quad (6)$$

where  $\rho_0 = m/2\pi h^2$  is the graphene bilayer density-of-states (per spin and valley) and the integral is carried out in the momentum shell  $-s < q < s$ . In the zero temperature limit

$$\chi_D^{ZS} = \frac{2_D}{h^2} \int_{-s}^s \frac{d^2 q}{(2\pi)^2} \frac{\tanh(\epsilon_q/2)}{4\epsilon_q} \xrightarrow{T \rightarrow 0} \frac{1}{2} \rho_0 \ln(s); \quad (7)$$

The ZS' channel shown in Fig. 4 corresponds to repeated interaction between a T particle and a B hole. This loop diagram involves only particle-propagation that is diagonal in interaction labels; its evaluation for the 1DES and graphene bilayers correspond closely. This is the channel responsible for the 1DES mean-field CDW instability<sup>4</sup> in which coherence is established between R and L particles<sup>5</sup>. In both cases it has the effect of enhancing repulsive interactions. We find

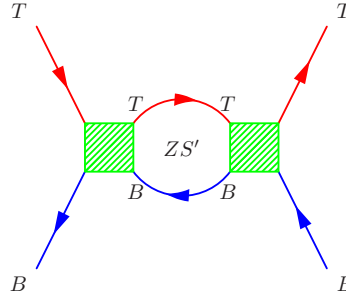


FIG. 4: ZS' loop correction in the one-loop perturbative RG.

$$\chi_D^{ZS'} = \frac{2_D}{h^2} \int_{-s}^s \frac{d^2 q}{(2\pi)^2} \chi \mathcal{G}_s^2(\mathbf{q}; i\epsilon_n) = \frac{2_D}{h^2} \int_{-s}^s \frac{d^2 q}{(2\pi)^2} \frac{\tanh(\epsilon_q/2)}{4\epsilon_q} = \frac{1}{2} \frac{2_D}{h^2} \rho_0 \ln(s); \quad (8)$$

The BCS loop corresponds to repeated interaction between the two incoming particles. In the 1DES case the contribution from this loop (see Fig. 5) cancels the ZS' contribution<sup>4</sup>, leading to marginal interactions and Luttinger liquid behavior. This same kind of BCS correction for graphene bilayer reads

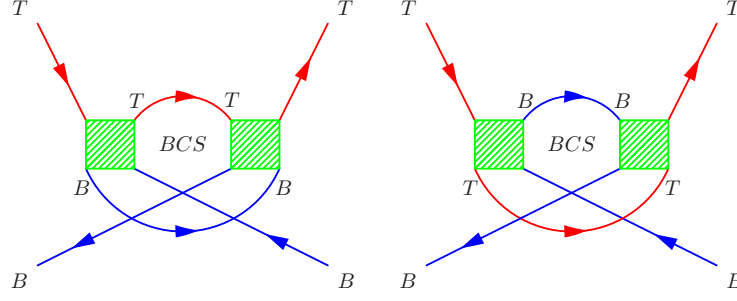


FIG .5: BCS (particle-particle) loop correction for singlet propagation in the one-loop perturbative RG calculation.

$$\begin{aligned}
 \text{BCS}_D^1 &= \frac{1}{2} \frac{2}{\hbar^2} \int^Z \frac{d^2 q}{(2\pi)^2} \sum_{i_n} \mathcal{G}_s(q; i_n) \mathcal{G}_s(-q; -i_n) \\
 &= \frac{1}{2} \frac{(2D)^2}{\hbar^2} \int^Z \frac{d^2 q}{(2\pi)^2} \sum_{i_n} \mathcal{G}_s(q; i_n) \mathcal{G}_s(-q; -i_n) \\
 &= \frac{1}{2} \frac{2D}{\hbar^2} \ln(s) :
 \end{aligned} \tag{9}$$

In the graphene bilayer case, however, there is an additional contribution (see Fig. 6) to the BCS loop contribution in which the incoming T and B particles both change layer labels before the second interaction. This contribution is possible because of the triplet layer pseudospin propagation and, in light of Eq. (5), gives a BCS contribution of opposite sign to the normal contribution:

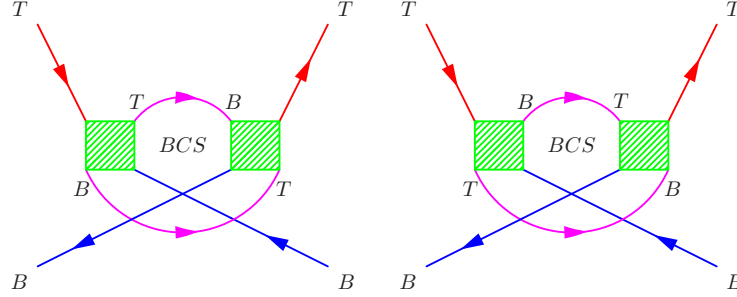


FIG .6: BCS (particle-particle) loop correction for triplet propagation in the one-loop perturbative RG calculation.

$$\begin{aligned}
 \text{BCS}_D^2 &= \frac{1}{2} \frac{2D(2D)}{\hbar^2} \int^Z \frac{d^2 q}{(2\pi)^2} \sum_{i_n} \mathcal{G}_t(q; i_n) \mathcal{G}_t(-q; -i_n) \\
 &= \frac{1}{2} \frac{(2D)^2}{\hbar^2} \int^Z \frac{d^2 q}{(2\pi)^2} \sum_{i_n} \mathcal{G}_t(q; i_n) \mathcal{G}_t(-q; -i_n) \\
 &= \frac{1}{2} \frac{2D}{\hbar^2} \ln(s) :
 \end{aligned} \tag{10}$$

It follows that the BCS loop contribution is absent in the graphene bilayer case because

$$\text{BCS}_D = \text{BCS}_D^1 + \text{BCS}_D^2 = 0 : \tag{11}$$

Therefore, at one-loop level, the renormalization of interlayer interaction is

$$\text{one loop}_D = \frac{ZS}{D} + \frac{ZS^0}{D} + \text{BCS}_D = \frac{2}{D} \ln(s) ; \tag{12}$$



which leads to the RG flow equation

$$\frac{d V_D}{d \ln(s)} = \frac{V_D^2}{D} : \quad (13)$$

Combined with the bare interlayer interaction  $V_D$  and integrating the flow equation we obtain that

$$V_D = \frac{V_{D0}}{1 - V_{D0} \ln(s)} \quad (14)$$

which diverges at the point  $V_{D0} = 1/\ln(s)$ .

For the Feynman diagrams drawing conventions we have chosen, the interaction correction to the layer pseudospin response function  $\chi_{zz}$ , which diverges at the pseudospin ferromagnet phase boundary, is obtained by closing the scattering function with a  $\chi_z$  vertex at top and bottom. The  $\chi_z$  operator measures the charge difference between T and B layers. Because it is an effective single-particle theory, fermion mean-field theory<sup>3</sup> corresponds to response function diagrams with at most a single particle-hole pair. It follows that mean-field theory is equivalent to a single-loop PRG calculation in which the BCS and ZS' channels are neglected and only the ZS channels is retained. In mean-field theory<sup>3</sup> the ideal graphene bilayer has an instability to a state in which charge is spontaneously transferred between the layers which is signalled by the divergence of  $\chi_{zz}$ . The PRG analysis demonstrates that the mean-field theory instability is enhanced by reinforcing ZS' channel contribution.

#### IV. PRG ANALYSIS FOR SPINFUL AND VALLEYFUL GRAPHENE BILAYERS

As discussed at the end of section II, there are ten interaction parameters for the spinful and valleyful case. The one-loop flow equations are derived in the same way as in the spinless valleyless case, except for the necessity of keeping track of the many possible configurations of the end labels on the loop propagators. We find that

$$\begin{aligned} \frac{d V_{SSD}}{d \ln(s)} &= \frac{1}{2} V_{SSD}^2 - V_{SSD} (V_{DSD} + V_{SSD}) - (V_{DD S} + V_{SD S}) (V_{DD D} + V_{SD D}) + \frac{1}{2} (V_{XSD} + V_{SSD})^2 \\ \frac{d V_{SDS}}{d \ln(s)} &= \frac{1}{2} V_{SDS}^2 - V_{SSD} (V_{DD S} + V_{SD S}) - (V_{DSD} + V_{SSD}) (V_{DD D} + V_{SD D}) + \frac{1}{2} (V_{XDS} + V_{SD S})^2 \\ \frac{d V_{SDD}}{d \ln(s)} &= \frac{1}{2} V_{SDD}^2 - V_{SSD} (V_{DD D} + V_{SD D}) - (V_{DSD} + V_{SSD}) (V_{DD S} + V_{SD S}) + \frac{1}{2} (V_{XDD} + V_{SD D})^2 \\ \frac{d V_{DSS}}{d \ln(s)} &= V_{DSS}^2 + \frac{1}{2} (V_{DSD} + V_{SSD})^2 + \frac{1}{2} (V_{DD S} + V_{SD S})^2 + \frac{1}{2} (V_{DD D} + V_{SD D})^2 + \frac{1}{2} V_{XSD}^2 + \frac{1}{2} V_{XDS}^2 + \frac{1}{2} V_{XDD}^2 \\ \frac{d V_{DSD}}{d \ln(s)} &= \frac{1}{2} V_{DSD}^2 + V_{SSD} (V_{DSD} + V_{SSD}) + (V_{DD D} + V_{SD D}) (V_{DD S} + V_{SD S}) - \frac{1}{2} (V_{DSD} + V_{XSD})^2 \\ \frac{d V_{DD S}}{d \ln(s)} &= \frac{1}{2} V_{DD S}^2 + V_{SSD} (V_{DD S} + V_{SD S}) + (V_{DD D} + V_{SD D}) (V_{DSD} + V_{SSD}) - \frac{1}{2} (V_{DD S} + V_{XDS})^2 \\ \frac{d V_{DD D}}{d \ln(s)} &= \frac{1}{2} V_{DD D}^2 + V_{SSD} (V_{DD D} + V_{SD D}) + (V_{DD S} + V_{SD S}) (V_{DSD} + V_{SSD}) - \frac{1}{2} (V_{DD D} + V_{XDD})^2 \\ \frac{d V_{XSD}}{d \ln(s)} &= V_{SSD} V_{XSD} - V_{XDS} V_{XDD} - \frac{1}{2} (V_{XSD} + V_{SSD})^2 - \frac{1}{2} (V_{XSD} + V_{DSD})^2 \\ \frac{d V_{XDS}}{d \ln(s)} &= V_{SSD} V_{XDS} - V_{XSD} V_{XDD} - \frac{1}{2} (V_{XDS} + V_{SD S})^2 - \frac{1}{2} (V_{XDS} + V_{DD S})^2 \\ \frac{d V_{XDD}}{d \ln(s)} &= V_{SSD} V_{XDD} - V_{XSD} V_{XDS} - \frac{1}{2} (V_{XDD} + V_{SD D})^2 - \frac{1}{2} (V_{XDD} + V_{DD D})^2 \end{aligned} \quad (15)$$

The only fixed point that we have identified is the non-interacting one. These ten coupled flow equations can be integrated numerically starting from bare interactions. In order to represent the property that same layer interactions will be slightly stronger than different layer interactions we set the bare interactions values to 1:1, 0.9 and 0 for  $V_{SSD}$  ( $V_{SDS}$ ,  $V_{SDD}$ ),  $V_{DSS}$  ( $V_{DSD}$ ;  $V_{DD S}$ ;  $V_{DD D}$ ) and  $V_{XSD}$  ( $V_{XDS}$ ;  $V_{XDD}$ ), respectively. (The motivation for this choice is explained in the next section.) We find that the interaction parameters flow away from the non-interacting fixed point and diverge at a finite value of  $s$  as illustrated in Fig. 7. The instability criterion implied by this one-loop PRG calculation is  $V_{D0} > 0.6/\ln(s)$ . The instability tendency is therefore enhanced by the spin and valley degrees of freedom since the criterion was  $V_{D0} > 1/\ln(s)$  for the spinless and valleyless case.

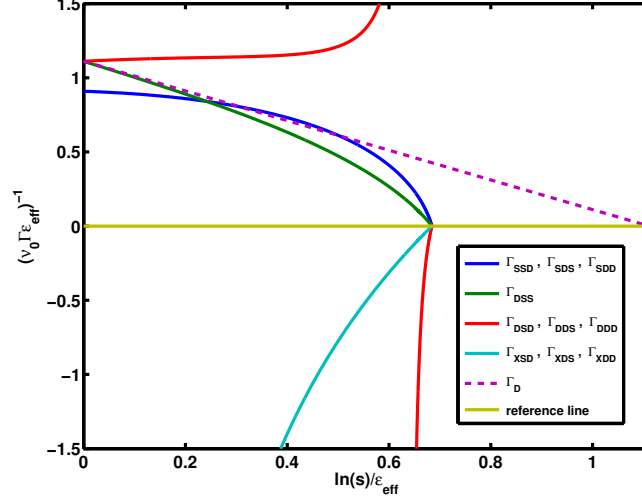


FIG. 7: Renormalized interaction flow. This illustration plots the inverse interaction strength  $(V_0 \epsilon_{eff})^{-1}$  versus the scaling parameter  $\ln(s)/\epsilon_{eff}$ .  $\epsilon_{eff}$  is the effective dielectric constant of the graphene bilayer and  $\epsilon_{vacuum} = \epsilon_{eff}$ . Interlayer interaction parameters  $\Gamma_{DSS}$  (green) and  $\Gamma_{XSD}; \Gamma_{XDS}; \Gamma_{XDD}$  (cyan) flow to large values most quickly. According to this estimate the normal state becomes unstable for  $V_D$  larger than  $\epsilon_{eff}^{-1} \approx 0.6 = \ln(s)$ .

## V. BARE INTERACTIONS AND THE TRIGONAL-WARPING EFFECT

The conclusions which can be drawn from the PRG calculation presented here are sensitive to the upper and lower momentum and energy cutoffs, which limit the applicability of the massive chiral fermion model for bilayer graphene, and to the strength of bare electron-electron scattering amplitudes. Below we estimate the range of  $s$  over which the RG flows discussed above apply, and the strength of the bare interaction  $V_0$ . We caution that, given the nature of the PRG calculations, the estimates presented below should be regarded as qualitative.

In practice the upper cutoff is the interlayer hopping energy  $t_1 \approx 0.4$  eV; at higher energies it is essential to account for two sublattice sites in each layer. We have in addition ignored the trigonal-warping part in the full Hamiltonian, due to a direct hopping process between the low-energy sites which has energy scale<sup>6,7</sup>  $t_3 \approx 0.3$  eV. Inserting the expression<sup>1</sup> for the effective mass of the massive chiral Fermion model we find that the model we have studied is appropriate for

$$\hbar v_F q_0 \frac{3}{2} = \frac{\hbar^2 q_0^2}{2m} = \frac{\hbar^2 q_0^2 v_F^2}{1} \quad (16)$$

where  $v_F \approx 10^8$  cm/s is the Fermi velocity near the Dirac point in the single-layer-graphene continuum model, and  $\epsilon_0 \approx 3$  eV is the intralayer near neighbor hopping energy. It follows that the high energy momentum cutoff  $q_H = q_1 = \hbar v_F$  and that the low energy momentum cutoff  $q_L = (q_1 = 0) = \hbar v_F$ , which gives the maximum value of the scaling parameter  $\ln(s)$ . Using accepted values for the hopping parameters<sup>6,7</sup>, it follows that the scaling relations we derive should apply approximately over a wavevector range corresponding to  $\ln(s)_{max} = \ln(q_H = q_L) - \ln(\epsilon_0 = 3) \approx 2.3$ .

We estimate the strength of the bare scattering amplitudes by evaluating the 2D Coulomb scattering potential at the cut-off wavevector  $k_H$ :

$$V_S \approx \frac{m}{2 \hbar^2} \frac{2 e^2}{k_H} = \frac{ee}{2} \quad (17)$$

where  $ee = e^2/\hbar v_F \approx 2.2$  is graphene's fine structure constant. The value used for  $V_S$  in the RG flows is motivated by this estimate. The value used for  $V_D$  is reduced by a factor of  $\exp(-k_H d)$  compared to  $V_S$  to account for the layer separation  $d \approx 3.35$  Å.

According to these estimates the bare value of  $V_D$  exceeds the stability limit of  $\epsilon_{eff}^{-1} \approx 0.6 = \ln(s)_{max} \approx 0.25$  by approximately a factor of four. The above estimates are for the case of a graphene bilayer in vacuum. For graphene layers on the surface of a substrate with dielectric constant  $\epsilon$ , interactions are expected to be reduced by a factor of  $(\epsilon + 1)/2$ . In the case of  $\text{SiO}_2$  substrates  $\epsilon \approx 4$  and the interaction strength exceeds the stability limit by a much

narrower margin. We expect that additional screening effects from graphene orbitals, which are normally neglected in continuum model calculations, will reduce interaction strengths at wavevectors near  $k_H$  somewhat and favor stable bilayers.

- 
- <sup>1</sup> McCann, E. & Fal'ko, V. I. Landau-level degeneracy and quantum hall effect in a graphite bilayer. *Phys. Rev. Lett.* 96, 086805 (2006).
  - <sup>2</sup> Min, H. & MacDonald, A. H. Chiral decomposition in the electronic structure of graphene multilayers. *Phys. Rev. B* 77, 155416 (2008).
  - <sup>3</sup> Min, H., Borghi, G., Polini, M. & MacDonald, A. H. Pseudospin magnetism in graphene. *Phys. Rev. B* 77, 041407(R) (2008).
  - <sup>4</sup> Shankar, R. Renormalization-group approach to interacting fermions. *Rev. Mod. Phys.* 66, 129 (1994).
  - <sup>5</sup> Giamarchi, T. *Quantum Physics in One Dimension* (Clarendon Press, Oxford, 2003).
  - <sup>6</sup> Castro Neto, A. H., Guinea, F., Peres, N. M. R., Novoselov, K. S. & Geim, A. K. The electronic properties of graphene. *Rev. Mod. Phys.* 81, 109 (2009).
  - <sup>7</sup> Koshino, M. & Ando, T. Transport in bilayer graphene: Calculations with in a self-consistent Born approximation. *Phys. Rev. B* 73, 245430 (2006).